Journal of Image Processing Theory and Applications (2025)
Clausius Scientific Press, Canada

DOI: 10.23977/jipta.2025.080104
ISSN 2560-6239 Vol. 8 Num. 1

CBBGAN: a color-blur balanced generation adversarial network for underwater image enhancement

Haiyang Yao[1,a], Ruige Guo[1], Yueyue Huang[1], Yuzhang Zang[2], Xiaobo Zhao[3], Tao Lei[1], Haiyan Wang[1,4]

[1]School of Electronic Information and Artificial Intelligence, Shaanxi University of Science and Technology, Xi'an, 710016, China
[2]Engineering and Design Department, Western Washington University, Bellingham, WA, USA
[3]Department of Electrical and Computer Engineering, Aarhus University, 8200 Aarhus, Denmark
[4]School of Marine Science and Technology, Northwestern Polytechnical University, Xi'an, 710072, China
[a]yaohy1991@126.com
**Corresponding author*

Keywords: Underwater Image Enhancement, Multi-stage Residual, Feature Fusion, Generation Adversarial Network (GAN), Optical Images

Abstract: Underwater optical image processing has garnered significant attention in various underwater applications. However, the presence of particles and the attenuation characteristics of optics in underwater environments lead to color distortion, low contrast, and blurring in optical images. Image enhancement techniques play a crucial role in improving the effectiveness of underwater image processing. In this study, we propose a color-blur balanced generation adversarial network (CBBGAN) for enhancing underwater optical images. CBBGAN aims to address color distortion and blurring issues. To address color distortion, we introduce the fusion-based Color Compensation module to mitigate color variations in the images. Then, the Multi-stage Residual based Generator is proposed to enhance the generative capacity of the Generative Adversarial Network (GAN), enabling the extraction of multi-dimensional features from the images. Furthermore, we propose a Structural Similarity based Joint Loss Function during the training phase, which is used to guide network training. We conducted qualitative analysis on different algorithms on three public datasets, which intuitively demonstrates that the proposed method effectively removes color deviation and blurring issues in images. In the quantitative experiment of EUVP, compared with the most advanced algorithms in PSNR and SSIM, CBBGAN has improved by 2 and 0.03, respectively. In addition, various indicators on the UFO and UIEB datasets also demonstrate the excellent performance of the CBBGAN algorithm.

1. Introduction

Underwater vision is crucial for Autonomous Underwater Vehicles (AUVs) in tasks like marine fishery, seabed mapping, and underwater exploration [1][2]. High-quality underwater images enhance detection and navigation, but imaging is challenged by turbulence, internal waves, irregular

scattering, and significant attenuation [3][4][5], leading to color distortion, blurring, and low contrast. These issues hinder AUV autonomy, making underwater image enhancement essential.

Enhancement methods fall into three categories: non-physical, physical model-based, and deep learning approaches. Non-physical methods adjust pixel values for visual improvement [6][7][8], but often introduce excessive distortion[9][10][11]. Physical model-based methods estimate image degradation parameters[12][13][14][15], yet struggle with complex underwater environments [16][17][18][19]. Deep learning has made significant progress[20][21][22][23][24], leveraging CNNs, GANs, and Transformers. CNNs extract local features[25][26][27][28], while GANs[29][30][31][32] and Transformers [33][34][35] capture global features. However, existing methods fail to balance color distortion and blurring effectively.

To address this, we propose a Color-Blur Balanced Generative Adversarial Network (CBBGAN) to optimize enhancement. The key contributions are:

(1) A Fusion-based color compensation module to mitigate color distortion using discriminator fusion for accurate correction.

(2) A Multi-stage Residual-based Generator to extract multi-dimensional features, improving detail retention.

(3) A Joint Loss Function integrating GAN loss, SSIM loss, and gradient loss to optimize both color fidelity and sharpness, ensuring superior enhancement results.

2. Materials and methods Methodology

2.1. Problem Description

The underwater physical environment, particularly in the ocean, presents distinctive challenges and disruptions to optical images, thus amplifying the complexities inherent in underwater image processing.

On one hand, longer-wavelength light is progressively absorbed with depth. The first to be absorbed is the red light. Beyond a depth of 20 meters, the majority of underwater scenes captured exhibit predominant hues of blue, green, and blue-green.

On the other hand, underwater environments are characterized by suspended particles, turbulence, and cavitation, which lead to irregular blurring, low contrast, and loss of details in images. Various types of optical components are present in underwater environments, resulting in scattering during image acquisition, including the direct component, the forward component, and the backward component, as depicted in Figure 1.

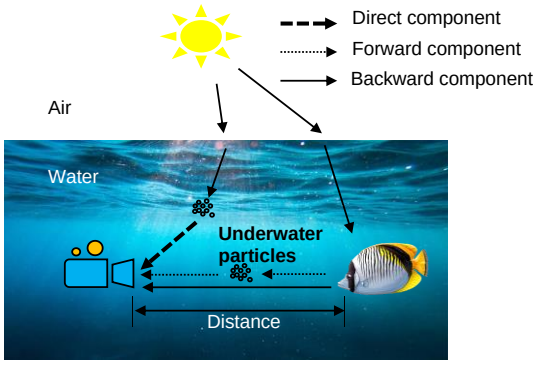

Figure 1: Light propagation characteristics underwater

2.2. CBBGAN Architecture

We have observed that although considerable work has been done to address the blue-green color cast and blurring issues in underwater images separately, there is still a lack of a satisfactory method that achieves a balance between these two aspects. To address this issue, this research paper introduces a Color-blur balanced Generation Adversarial Network (CBBGAN).

As shown in Figure 2, the CBBGAN learns the mapping between distorted and non-distorted underwater images, employing an end-to-end and data-driven training approach. The network comprises three main modules: Fusion-based Color Compensation module, Multi-stage Residual-based Generator module, and Structural Similarity-based multi-loss module.

2.2.1. Fusion based Color Compensation

Color variation is a common issue in underwater optical images, so the color compensation module is specifically designed to mitigate the impact of color cast. Firstly, the white balance method is employed to equalize the gray levels of the RGB channels[36]. For an input image I, the red compensation is achieved by:

$$I_{rc}(x) = I_r(x) + \alpha_r\left(\bar{I}_g - \bar{I}_r\right)\left(1 - I_r(x)\right)I_g(x) \tag{1}$$

where I_r and I_g are red and green channel of I, respectively. $\bar{I}_r$ and $\bar{I}_g$ are averages of Ir and Ig, $\alpha r=1$. And the blue compensation is realized by:

$$I_{bc}(x) = I_b(x) + \alpha_b\left(\bar{I}_g - \bar{I}_b\right)\left(1 - I_b(x)\right)I_g(x) \tag{2}$$

where I_b is blue channel of I, $\bar{I}_b$ is the averages of I_b, and $\alpha_b=1$.

Then, we perform Gamma correction and sharpening on the image. Gamma correction aims to increase the contrast and enhance the overall brightness of the image by expanding the range between dark and light regions. The gamma correction coefficient is obtained by learning.

The sharpening process is applied to reduce degradation caused by scattering and preserve fine details in the image. The sharpened image, denoted as S, is defined as:

$$S = \left(1 + M\left\{I - G * I\right\}\right)/2 \tag{3}$$

where M{.} represents the histogram stretching operation. This operation scales the intensity of all color pixels in the image, allowing the adjusted pixel values to cover the entire dynamic range.

Finally, the fused image is obtained by blending the initial color-corrected image with other processed versions of the image using a specific weight. This weight is the second learned parameter in this module and determines the contribution of each processed image to the final fused image. The optimal balance between color correction and other enhancement techniques can be achieved, resulting in improved and visually appealing images.

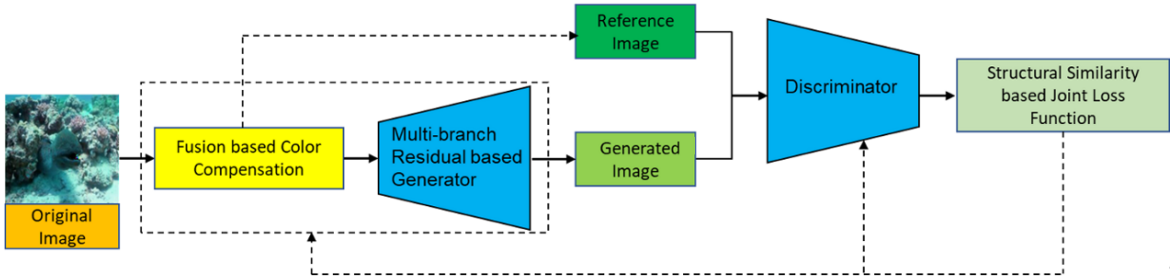

Figure 2: Frame of the CBBGAN

2.2.2. Multi-stage Residual-based Generator

The Generator comprises convolutional and deconvolutional layers, normalization layers, and activation layers in various configurations. However, the excessive use of deconvolution layers leads to the emergence of checkerboard artifacts in the generated images[37]. These artifacts occur due to uneven overlay during the deconvolution process, particularly when the kernel size is not evenly divisible by the step size. This uneven overlay is more pronounced in two-dimensional space. As shown in Figure 3, the deconvolution with a step size of 2 and a kernel size of 3 results in n－1 overlays of n inputs in one dimension. In two dimensions, the overlap becomes nearly four times, exacerbating the occurrence of checkerboard artifacts in the images. To mitigate this issue, one the one hand, we utilize two deconvolutions for feature image up-sampling. The feature input has a step size of 2 and uses a convolution layer with a kernel size of 3. Additionally, the up-sampling of the feature layer is further achieved through deconvolution with a step size of 2.

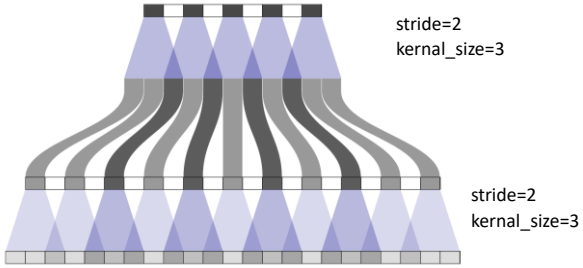

Figure 3: Uneven overlap of different dimensions

On the other hand, we found that the restriction of deconvolution sizes might decrease the feature diversity and learning capacity. We design a multi-stage residual convolution module (Muti-Conv). Muti-Conv utilizes a three-stage convolution structure to capture features at different levels in images and applies residual learning to maintain identity mapping between convolution layers. Each stage has convolution layer(s) and LeakyReLU activation(s). Images from the Fusion-based Color Compensation module perform two convolutions (first), generating two feature vectors, and the two features are combined to obtain stage one vector.

The stage one vector further performs a convolution and LeakyReLU module to obtain the stage two vector(second). The stage one vector and the stage two vector are fused utilizing a skip connection layer. Finally, the input feature and the output feature of the last convolution block(third) are combined using the residual principle. The convolution core size is set to 3x3, the stride is 2, and there are 128 channels, as shown in Figure 4.

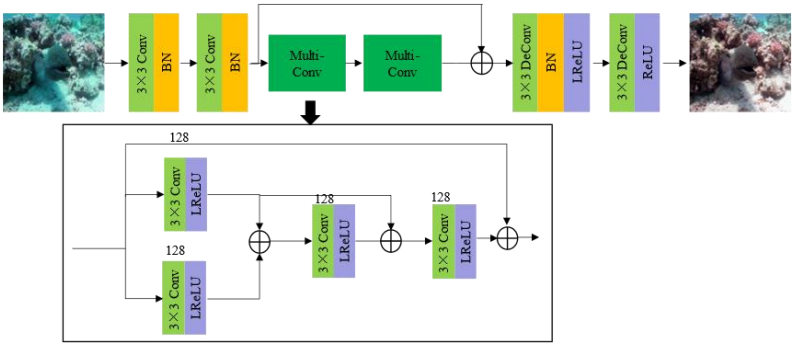

Figure 4: Architectures of generator networks. “Conv” denotes convolution layer, whereas “Deconv” denotes deconvolution layer. Muti-Conv represents Mixed-convolution Module and “BN” represents batch normalization.

2.2.3. Discriminator

The Discriminator distinguishes the differences between the images generated by the Generator and their corresponding reference images. The error calculated by the Discriminator is then used to provide feedback to each layer of the network. Through parameter updating, the Discriminator continuously improves its discrimination ability, resulting in the generated images becoming closer to the reference images. The Discriminator in this work adopts the PatchGAN architecture, as shown in Figure 5. It consists five convolution layers that are responsible for down-sampling. The inputs to the Discriminator are the image from Generator, and its corresponding reference image. Each input image is divided into multiple patches, with a size of 4x4 pixels. The convolution layers have a kernel size of 2 and the channel numbers are set to 64, 128, 256, and 512 respectively. Nonlinear transformation is applied using the LeakyReLU activation function with a parameter of 0.2.

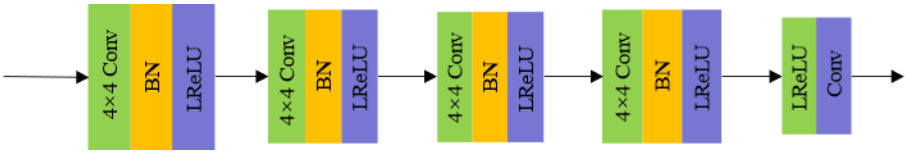

Figure 5: Architecture of Discriminator networks, Spectral normalization is used in the convolution layer of the discriminator.

2.3. Joint Loss Function

We introduce the joint loss function that incorporates multiple components, including GAN loss, SSIM loss, and gradient loss, to achieve the balance between color-accuracy and clarity in the enhanced images.

2.3.1. Adversarial Loss

For the mapping function G: X→Y, the adversarial loss can be expressed as :

$$L_{GAN} = E_{x \sim p_{data}(x)}\left[\log D(x)\right] + E_{y \sim p_{noise}(y)}\left[\log\left(1 - D\left(G(y)\right)\right)\right] \tag{4}$$

where X is the set of original images and Y is the noise image, D(•) is the Discriminator, G(•) is the Generator.

2.3.2. SSIM Loss

Generally, MSE loss is susceptible to light interference. By contrast, Structural Similarity Index Measure (SSIM) loss has better performance and retains the content and structure of the image. The SSIM loss between the generated image and the real image is defined as:

$$SSIM(x,y) = \frac{\left(2\mu_x\mu_y + C_1\right)\left(2\sigma_{xy} + C_2\right)}{\left(\mu_x^2 + \mu_y^2 + C_1\right)\left(\sigma_x^2 + \sigma_y^2 + C_2\right)} \tag{5}$$

where μ_x prepresents the average pixel size of the generated image, σ_x is the standard deviation of the generated image pixel, μ_y is the average pixel size of the real image, and σ_y represents the standard deviation of the real pixel. C_1=0.02 and C_2=0.03 are constant values. Then, the SSIM value of each pixel between the real image X' and the converted image G(x) can be calculated by:

$$L_{SSIM}\left(X',G(x)\right)=1-\frac{1}{N}\sum_{p=1}^{N}\left(SSIM\left(x,y\right)\right) \tag{6}$$

2.3.3. Gradient Penalty Loss

To address the issue of blurry images commonly generated by the Generator, we directly penalize the differences in image gradient predictions within the Generator. This approach helps to enhance the quality of these images by encouraging sharper edges and finer details. The gradient penalty loss is formulated as:

$$\begin{aligned} L_{GDL}\left(I^{C},I^{P}\right)=\sum_{i,j}&\left\|\left|I_{i,j}^{C}-I_{i-1,j}^{C}\right|-\left|I_{i,j}^{P}-I_{i-1,j}^{P}\right|\right\|^{\alpha} \\ &+\left\|\left|I_{i,j-1}^{C}-I_{i,j}^{C}\right|-\left|I_{i,j-1}^{P}-I_{i,j}^{P}\right|\right\|^{\alpha} \end{aligned} \tag{7}$$

where I^C is the reference image, I^O is the original image, $I^P=G(I^O)$, α is a number greater than 1.

2.3.4. Total Loss

Combining the above three losses, the Joint loss function is:

$$L_{CBBGAN}=\gamma L_{GAN}(G,D)+L_{SSIM}(G)+L_{GDL} \tag{8}$$

where the loss weight $\gamma = 2$ is an empirically tuned hyper-parameter. The optimization of Discriminator is maximized by (4), and the optimization of Generator is minimized by (6), respectively.

3. Experiment Setting

In this section, firstly, we explore the underwater image datasets used in this paper. Secondly, we discuss the evaluation index of the generated image and the specific parameter settings of the experiment. Then, we introduce our test datasets.

3.1. Training and Validation Datasets

We conducted experiments on multiple publicly available datasets, including both reference-based learning effectiveness tests and non-reference generalization experiments. The EUVP dataset[22] comprises a vast collection of ocean images which captures under diverse visibility conditions[38]. The UIEB dataset[21] consists 890 underwater images of various lighting conditions and their corresponding references. Additionally, we incorporate the UFO-120 dataset[39], which comprises 1500 paired training underwater images and 120 unpaired testing images. This dataset offers a diverse range of underwater scenes, and serves as a valuable resource for evaluating the generalization capability of our proposed method.

3.2. Evaluation Metrics

To assess the quality of our results, we employ several evaluation metrics. To compare the enhanced images with their corresponding reference images, we utilize the Peak Signal-to-Noise Ratio (PSNR)[40] and SSIM[41]. The PSNR metric evaluates the dissimilarity between the enhanced image and the reference image by the mean square error (MSE). The SSIM evaluates the similarity between the two images from brightness, contrast and structure.

We employ Underwater Image Quality Measure (UIQM)[42] and Underwater Color Image Quality Evaluation (UCIQE)[43] to evaluate the quality of non-reference images. The UIQM metric

takes into account Underwater Image Colorfulness (UICM), Underwater Image Sharpness Measure (UISM), and Underwater Image Contrast Measure (UIConM). The UCIQE metric evaluates the color quality of underwater images by considering the color density, saturation, and contrast based on the CIELab color space.

3.3. Parameters setting

The training and test images are resized to a size of 256×256×3. The Leaky Rectified Linear Unit (LReLU) activation function is utilized with a slope of 0.2. The Adam optimization algorithm is employed with an initial learning rate of 0.0002. The batch size for training is set to 16. Notably, the Discriminator is updated 5 times for each update of the Generator. The training process is performed for 100 epochs using the paddle framework on the Tesla V100 platform.

3.4. Test Datasets

The first test set is derived from a subset of the EUVP dataset, which includes diverse images captured in various water bodies. The second test set consists fuzzy images from the UFO-120 dataset. The third test set is obtained from a portion of the UIEB dataset, which encompasses images captured under different lighting conditions and exhibiting a wide range of colors. These test sets are selected to assess the model's performance under different underwater imaging scenarios.

4. Results

In this section, we present a comprehensive analysis and comparison of the experimental results obtained from various underwater image enhancement algorithms, including both traditional and state-of-the-art deep learning approaches. Our evaluation includes eleven algorithms for comparison: two non-physical model-based methods, GC[44] and HE[45]; two physical model-based methods, UDCP[46] and IBLA[17]; seven state-of-the-art depth learning methods UWGAN[22], Shallow-UWNet[26], FGAN[31], U-Shape Transformer[33], NU2Net[47], SFGNet and P2CNet[28].

We conduct both subjective and objective assessments to evaluate our network. The subjective evaluation involved visual comparisons of color accuracy and contrast in the enhanced images. The objective evaluation relied on metrics above, which provide quantifiable measures of image quality, color richness, sharpness, and contrast.

The analysis and comparison of the experiment results enable us to assess the strengths and weaknesses of various underwater image enhancement methods and provided empirical support for the efficacy of our proposed CBBGAN approach.

4.1. Qualitative Evaluation

The qualitative evaluation results are presented in Figure 6-8 on three datasets: EUVP, UFO-120, and UIEB. GC fails to remove water mist, resulting in degraded image quality. HE tends to produce excessively bright images, leading to the loss of important details in dark regions. The two physics-based methods exhibit limitations in removing color deviations. UDCP improves image contrast, but lead to oversaturation issues and overall darkening. IBLA also fails to address color biases and results in darker images.

Shallow-UWnet enhances the overall brightness of images, but tends to amplify the presence of underwater fog. FGAN and U-Shape perform better than Shallow-UWnet in removing water mist, while UWGAN still struggles to effectively correct color deviations in some images. NU2Net

performs poorly in addressing color cast issues in underwater images. P2CNet restores the color of the image, but is unable to completely remove the blur. In comparison, the CBBGAN demonstrates clearer image enhancement results with preserved details. It notably improves the overall color saturation and clarity of the images in the test set, surpassing other existing algorithms in terms of subjective evaluation. These results indicate the subjective superiority of the proposed algorithm over the other compared algorithms in underwater image enhancement

Figure 6: Enhanced results of different methods in test set EUVP

Figure 7: Enhanced results of different methods in test set UFO-120

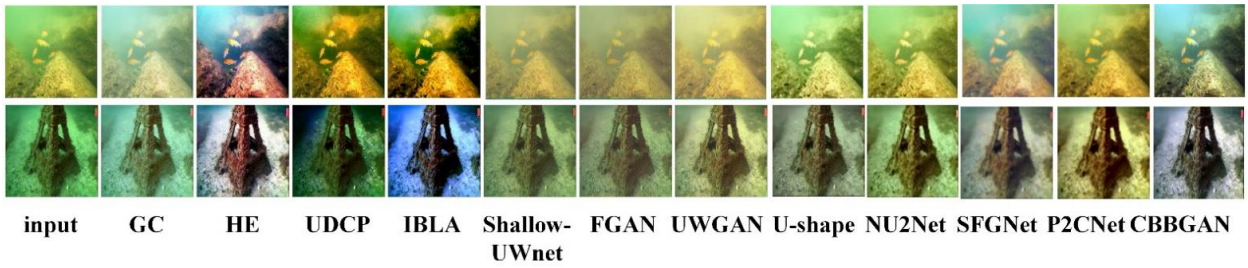

Figure 8: Enhanced results of different methods in test set UIEB

4.2. Quantitative Evaluation

The results of different methods on the EUVP dataset are shown in Table 1. Compared to all deep learning methods, our approach achieved the best scores in PSNR, SSIM, and UCIQE, and received a suboptimal score in UIQM. PSNR and SSIM have increased by 0.035 and 1.766 respectively compared to the second place. Note: Red represents the highest score and blue represents the second highest score.

As indicated in Table 2, facing the new underwater environment dataset UIEB, our method performed poorly in PSNR and SSIM, but achieved good scores in UIQM and UCIQE. Meanwhile, as shown in Fig.8, our method demonstrates the best visual performance in both removing color deviation and blurring.

Table 1: Results of different methods on test set EUVP

	SSIM	PSNR	UIQM	UCIQE
GC	0.764	16.229	2.82	0.37
HE	0.631	13.738	2.982	**0.501**
UDCP	0.574	14.519	1.857	**0.514**
IBLA	0.72	18.95	2.197	0.482
Shallow-UWnet	0.813	22.661	2.926	0.377
FGAN	**0.814**	**23.511**	3.036	0.386
UWGAN	0.796	21.155	**3.100**	0.406
U-Shape	0.805	22.354	3.012	0.403
NU2Net	0.804	20.36	2.879	0.434
SFGNet	0.812	20.42	2.890	0.448
P2CNet	0.795	20.95	2.879	0.434
CBBGAN	**0.849**	**25.277**	**3.065**	**0.436**

Table 2: Results of different methods on test set UIEB

	SSIM	PSNR	UIQM	UCIQE
GC	0.743	15.572	2.586	0.336
HE	0.789	16.606	2.921	0.507
UDCP	0.494	10.902	1.802	**0.513**
IBLA	0.666	15.602	1.833	0.472
Shallow-UWnet	0.721	16.384	2.968	0.319
FGAN	0.681	15.714	3.097	0.318
UWGAN	0.706	15.76	**3.196**	0.371
U-Shape	**0.801**	**20.181**	2.983	0.432
NU2Net	**0.767**	**19.612**	2.932	0.426
SFGNet	0.715	18.136	3.005	0.442
P2CNet	0.779	18.818	2.874	0.396
CBBGAN	**0.752**	**16.711**	**3.104**	**0.514**

Table 3: Results of different methods on test set Test-U and UFO-120

	Test-U		UFO-120	
	UIQM	UCIQE	UIQM	UCIQE
GC	0.743	15.572	2.586	0.336
HE	0.789	16.606	2.921	0.507
UDCP	0.494	10.902	1.802	**0.513**
IBLA	0.666	15.602	1.833	0.472
Shallow-UWnet	0.721	16.384	2.968	0.319
FGAN	0.681	15.714	3.097	0.318
UWGAN	0.706	15.76	**3.196**	0.371
U-Shape	**0.801**	**20.181**	2.983	0.432
NU2Net	**0.767**	**19.612**	2.932	0.426
SFGNet	0.715	18.136	3.005	0.442
P2CNet	0.779	18.818	2.874	0.396
CBBGAN	**0.752**	**16.711**	**3.104**	**0.514**

We utilize the UIQM and UCIQE metrics to quantitatively evaluate the performance of different

methodologies, and employ a reference-free test set consisting of 60 images from the UIEB and UFO-120 datasets. As illustrated in Table 3, the proposed method exhibits robust performance, attaining superior results in both UIQM and UCIQE.

These results validate the effectiveness of the proposed method in enhancing image quality, color representation, and overall visual perception, even in the non-reference images. The CBBGAN acquires the ability of balancing the color saturation and clarity in image enhancement.

4.3. Ablation Study

In order to assess the impact of the Color Compensation, Multi-Conv module and the Joint loss function on the ability of the image enhancement, ablation studies are conducted on three different datasets: EUVP, UFO-120, and UIEB. These studies compare the performance of the base model (Patch GAN) with the enhanced model with Multi-Conv module, Color Compensation and the CBBGAN.

Table 4 indicates that, across the three datasets, the Color Compensation improves the image quality metrics to a certain extent. And the Multi-Conv module consistently exhibited improvements in image quality metrics compared to the base model. The Multi-Conv module demonstrates enhancements in SSIM, PSNR, and UIQM, highlighting its effectiveness in enhancing image quality. Furthermore, the CBBGAN also displays significant improvements in terms of SSIM, PSNR, UIQM and UCIQE in both UFO-120 and UIEB, verifying the effectiveness of the Joint loss function designed in this paper.

Table 4: Quantitative results of each module on EUVP, UFO-120 and UIEB

Test set	Index	Base	Base+ Color	Base+ Multi	CBBGAN
EUVP	**SSIM**	0.831	0.837	0.849	**0.849**
	PSNR	23.440	24.249	25.252	**25.277**
	UIQM	2.864	2.831	2.809	**3.065**
	UCIQE	0.426	0.427	0.429	**0.426**
UFO-120	**SSIM**	0.760	0.778	0.785	**0.796**
	PSNR	22.250	23.374	24.479	**24.591**
	UIQM	2.823	2.791	2.801	**2.996**
	UCIQE	0.427	0.429	0.434	**0.441**
UIEB	**SSIM**	0.725	0.731	0.735	**0.752**
	PSNR	16.330	16.470	16.573	**16.711**
	SSIM	0.831	0.837	0.849	**0.849**
	PSNR	23.440	24.249	25.252	**25.277**

5. Conclusion

In this paper, we build a Color-Blur Balanced Generation Adversarial network (CBBGAN) for underwater image enhancement. The CBBGAN aims to strike a balance between addressing color distortion and blurring issues. In order to address the color cast and blur issues in underwater optical images, we develop a Fusion based Color Compensation module, which aims to reduce color variation. Additionally, a Multi-stage Residual based Generator in the GAN framework is designed to extract multi-dimensional features from images. To enhance the effectiveness of the model in addressing color cast and blur issues, we design a Joint Loss Function.

Experimental results on three public datasets, EUVP, UFO-120, and UIEB, demonstrate that our proposed method, CBBGAN, outperforms typical and state-of-the-art methods in terms of four key

indicators. The results show that CBBGAN is capable of producing high-quality underwater optical images, which in turn can improve the efficiency of AUV underwater tasks.

References

[1] R. Liu, X. Fan, M. Zhu, et al., "Real-World Underwater Enhancement: Challenges, Benchmarks, and Solutions Under Natural Light," IEEE Trans Circuits Syst Video Technol, vol. 30, no. 12, pp. 4861-4875, Dec. 2020.

[2] O. K. Soni and J. S. Kumare, "A Survey on Underwater Images Enhancement Techniques," 2020 IEEE 9th International Conference on Communication Systems and Network Technologies (CSNT), Gwalior, India, 2020, pp. 333-338.

[3] Q. Jiang, Y. Gu, C. Li, et al., "Underwater Image Enhancement Quality Evaluation: Benchmark Dataset and Objective Metric," IEEE Trans Circuits Syst Video Technol, vol. 32, no. 9, pp. 5959-5974, Sept. 2022.

[4] Q. Qi et al., "Underwater Image Co-Enhancement with Correlation Feature Matching and Joint Learning," IEEE Trans Circuits Syst Video Technol, vol. 32, no. 3, pp. 1133-1147, March 2022.

[5] Z. Wang, L. Shen, Z. Wang, et al., "Generation-Based Joint Luminance-Chrominance Learning for Underwater Image Quality Assessment," IEEE Trans Circuits Syst Video Technol, vol. 33, no. 3, pp. 1123-1139, March 2023.

[6] C. Ancuti, C. O. Ancuti, T. Haber and P. Bekaert, "Enhancing underwater images and videos by fusion," in CVPR, Providence, RI, USA, 2012, pp. 81-88.

[7] X. Fu, Z. Fan, M. Ling, Y. Huang and X. Ding, "Two-step approach for single underwater image enhancement," ISPACS, Xiamen, China, 2017, pp. 789-794

[8] Iqbal K , Salam R A , Osman A , et al. Underwater image enhancement using an integrated colour model[J]. IAENG Int J Comput Sci, 2007, 34(2): 239--244.

[9] Chen Zhao, Weiling Cai, Chenyu Dong, Ziqi Zeng, "Toward Sufficient Spatial-Frequency Interaction for Gradient-aware Underwater Image Enhancement", ICASSP 2024.

[10] K. Iqbal, M. Odetayo, A. James, Rosalina Abdul Salam and Abdullah Zawawi Hj Talib, "Enhancing the low-quality images using Unsupervised Colour Correction Method," IEEE SMC, Istanbul, Turkey, 2010, pp. 1703-1709.

[11] H. Qiang, Y. Zhong, Y. Zhu, X. Zhong, Q. Xiao and S. Dian, "Underwater Image Enhancement Based on Multichannel Adaptive Compensation," in IEEE Transactions on Instrumentation and Measurement, vol. 73, pp. 1-10, 2024, Art no. 5014810.

[12] X. Fu, P. Zhuang, Y. Huang, Y. Liao, X. -P. Zhang and X. Ding, "A retinex-based enhancing approach for single underwater image," ICIP, Paris, France, 2014, pp. 4572-4576.

[13] C. -Y. Li, J. -C. Guo, R. -M. Cong, Y. -W. Pang and B. Wang, "Underwater Image Enhancement by Dehazing With Minimum Information Loss and Histogram Distribution Prior," IEEE T Image Process, vol. 25, no. 12, pp. 5664-5677, Dec. 2016.

[14] N. Carlevaris-Bianco, A. Mohan and R. M. Eustice, "Initial results in underwater single image dehazing," MTS/IEEE OCEANS, Seattle, WA, USA, 2010, pp. 1-8.

[15] K. He, J. Sun and X. Tang, "Single Image Haze Removal Using Dark Channel Prior," IEEE Trans. Pattern Anal. Mach. Intell., vol. 33, no. 12, pp. 2341-2353, Dec. 2011.

[16] J. Y. Chiang and Y. -C. Chen, "Underwater Image Enhancement by Wavelength Compensation and Dehazing," IEEE T Image Process, vol. 21, no. 4, pp. 1756-1769, April 2012.

[17] Y. -T. Peng and P. C. Cosman, "Underwater Image Restoration Based on Image Blurriness and Light Absorption," IEEE T Image Process, vol. 26, no. 4, pp. 1579-1594, April 2017.

[18] Galdran A, Pardo D, Picón A, et al. Automatic red-channel underwater image restoration[J]. J Vis Commun Image Represent, vol: 26, pp: 132-145, Jan. 2015.

[19] P. L. J. Drews, E. R. Nascimento, S. S. C. Botelho and M. F. Montenegro Campos, "Underwater Depth Estimation and Image Restoration Based on Single Images," IEEE Comput. Graph Appl., vol. 36, no. 2, pp. 24-35, Apr. 2016.

[20] Y. Guo, H. Li and P. Zhuang, "Underwater Image Enhancement Using a Multiscale Dense Generative Adversarial Network," IEEE J. Ocean. Eng, vol. 45, no. 3, pp. 862-870, July 2020.

[21] C. Li et al., "An Underwater Image Enhancement Benchmark Dataset and Beyond," IEEE T Image Process, vol. 29, pp. 4376-4389, 2020.

[22] C. Fabbri, M. J. Islam and J. Sattar, "Enhancing Underwater Imagery Using Generative Adversarial Networks," ICRA, Brisbane, QLD, Australia, 2018, pp. 7159-7165.

[23] C. Li, J. Guo and C. Guo, "Emerging From Water: Underwater Image Color Correction Based on Weakly Supervised Color Transfer," IEEE Signal Process Lett., vol. 25, no. 3, pp. 323-327, March 2018.

[24] M. J. Islam, Y. Xia and J. Sattar, "Fast Underwater Image Enhancement for Improved Visual Perception," IEEE Robot. Autom. Lett, vol. 5, no. 2, pp. 3227-3234, April 2020.

[25] Y. Wang, J. Zhang, Y. Cao and Z. Wang, "A deep CNN method for underwater image enhancement," ICIP, Beijing,

China, 2017, pp. 1382-1386.
[26] N, Ankita, A Swarnakar, and K Mittal. "Shallow-uwnet: Compressed model for underwater image enhancement (student abstract)." AAAI. Vol. 35. No. 18. pp: 15853-15854, Jan. 2021.
[27] N. Qiao, J. Sun, Q. Ge and C. Sun, "UIE-FSMC: Underwater Image Enhancement Based on Few-Shot Learning and Multi-Color Space," in IEEE Transactions on Circuits and Systems for Video Technology, vol. 33, no. 10, pp. 5391-5405, Oct. 2023.
[28] Y. Rao, W. Liu, K. Li, H. Fan, S. Wang and J. Dong, "Deep Color Compensation for Generalized Underwater Image Enhancement," IEEE Transactions on Circuits and Systems for Video Technology, vol. 34, no. 4, pp. 2577-2590, April 2024.
[29] Goodfellow, Ian, et al. "Generative adversarial networks." Commun. ACM, vol: 63.no: 11 pp: 139-144, Nov. 2020.
[30] J. Li, K. A. Skinner, R. M. Eustice and M. Johnson-Roberson, "WaterGAN: Unsupervised Generative Network to Enable Real-Time Color Correction of Monocular Underwater Images," IEEE Robot. Autom. Lett, vol. 3, no. 1, pp. 387-394, Jan. 2018.
[31] Islam M J, Xia Y, Sattar J. Fast underwater image enhancement for improved visual perception[J]. IEEE Robotics and Automation Letters, 2020, 5(2): 3227-3234.
[32] P. Hambarde, S. Murala and A. Dhall, "UW-GAN: Single-Image Depth Estimation and Image Enhancement for Underwater Images," in IEEE Transactions on Instrumentation and Measurement, vol. 70, pp. 1-12, 2021, Art no. 5018412.
[33] L. Peng, C. Zhu and L. Bian, "U-Shape Transformer for Underwater Image Enhancement," in IEEE Transactions on Image Processing, vol. 32, pp. 3066-3079, 2023.
[34] Z. Huang, J. Li, Z. Hua and L. Fan, "Underwater Image Enhancement via Adaptive Group Attention-Based Multiscale Cascade Transformer," in IEEE Transactions on Instrumentation and Measurement, vol. 71, pp. 1-18, 2022, Art no. 5015618.
[35] M. Yang, Z. Xie, J. Dong, H. Liu, H. Wang and M. Shen, "Distortion-Independent Pairwise Underwater Image Perceptual Quality Comparison," in IEEE Transactions on Instrumentation and Measurement, vol. 72, pp. 1-15, 2023, Art no. 5024415.
[36] C. O. Ancuti, C. Ancuti, C. De Vleeschouwer and P. Bekaert, "Color Balance and Fusion for Underwater Image Enhancement," IEEE T Image Process, vol. 27, no. 1, pp. 379-393, Jan. 2018.
[37] A Odena, V Dumoulin, and C Olah. Deconvolution and checkerboard artifacts[J]. Distill, vol: 1, no: 10, e3.2016.doi: 10.23915/distill.00003.
[38] J. -Y. Zhu, T. Park, P. Isola and A. A. Efros, "Unpaired Image-to-Image Translation Using Cycle-Consistent Adversarial Networks," ICCV, Venice, Italy, 2017, pp. 2242-2251.
[39] M J Islam, , P Luo , J Sattar. Simultaneous Enhancement and Super-Resolution of Underwater Imagery for Improved Visual Perception, RSS 2020, Corvalis, Oregon, USA, Jul. 2020.
[40] M. Yang, J. Hu, and C. Li, et al. "An In-Depth Survey of Underwater Image Enhancement and Restoration," IEEE Access, vol. 7, pp. 123638-123657, Aug. 2019.
[41] Wang Z, Bovik A C, Sheikh H R, et al. Image quality assessment: from error visibility to structural similarity[J]. IEEE transactions on image processing, 2004, 13(4): 600-612.
[42] Yang M, Sowmya A. An underwater color image quality evaluation metric[J]. IEEE Transactions on Image Processing, 2015, 24(12): 6062-6071.
[43] Panetta K, Gao C, Agaian S. Human-visual-system-inspired underwater image quality measures[J]. IEEE Journal of Oceanic Engineering, 2015, 41(3): 541-551.
[44] H. Farid, "Blind inverse gamma correction," IEEE T Image Process, vol. 10, no. 10, pp. 1428-1433, Oct. 2001, doi: 10.1109/83.951529.
[45] Hummel R. Image enhancement by histogram transformation[J]. CVGIP, vol: 6, no.2, pp: 184-195, Apr. 1977.
[46] P. Drews Jr, E. do Nascimento, and F. Moraes et al. "Transmission Estimation in Underwater Single Images," ICCV, Sydney, NSW, Australia, 2013, pp. 825-830.
[47] Guo C, Wu R, Jin X, et al. Underwater ranker: Learn which is better and how to be better[C]//Proceedings of the AAAI conference on artificial intelligence. 2023, 37(1): 702-709.